DOI: 10.7641/CTA.2013.12041

基于Radau伪谱法的重复使用运载器再入轨迹优化

韩　鹏[†], 单家元

(北京理工大学 飞行动力学与控制教育部重点实验室, 北京 100081)

摘要: 为了提高数值解法的收敛速度, 本文利用Radau伪谱法求解重复使用运载器的再入轨迹优化问题. 该方法在一组Legendre-Gauss-Radau点上构造全局Lagrange插值多项式对状态变量和控制变量进行逼近, 在动力学方程中状态变量对时间的导数可由插值多项式的导数来近似, 故可将动力学方程约束转化为在Legendre-Gauss-Radau点上的代数微分方程约束. 因此, 可将连续时间的最优控制问题转化为有限维的非线性规划(NLP)问题, 之后通过稀疏NLP求解器SNOPT即可对其进行求解. 最后的仿真结果显示, 通过该方法优化后的再入轨迹成功满足过程约束与边界约束. 由于该方法的高效率和高精度特性, 可将其应用于轨迹快速优化工程实际问题中.

关键词: 重复使用运载器; 轨迹优化; 直接法; Radau伪谱法

中图分类号: V448.235　　　**文献标识码**: A

Re-entry trajectory optimization using Radau pseudospectral method

HAN Peng[†], SHAN Jia-yuan

(Key Laboratory of Dynamic and Control of Flight Vehicle, Ministry of Education,
Beijing Institute of Technology, Beijing 100081, China)

Abstract: To increase the convergence rate of the numerical method, we employ the Radau pseudospectral method (RPM) in solving the optimal re-entry trajectory for the reusable launch vehicle. In this method, a finite base of global Lagrange interpolating polynomials is used to approximate the states and control at a set of Legendre-Gauss-Radau points. The time derivative of the state in the dynamic equations is approximated by the derivative of the interpolating polynomial, therefore they can be converted to the differential-algebraic equations at the Legendre-Gauss-Radau points. Consequently, the continuous-time optimal control problem is transcribed to a finite-dimensional nonlinear programming (NLP) problem. Then, the resulting NLP problem is solved by a sparse nonlinear programming solver named SNOPT. Finally, simulation results show that the optimized re-entry trajectory satisfies the path constraints and the boundary constraints successfully. The results indicate that the RPM can be applied to fast trajectory-generation problems in practical engineering due to its high efficiency and high precision.

Key words: reusable launch vehicle; trajectory optimization; direct method; Radau pseudospectral method

1 Introduction

During the re-entry phase, the Reusable launch vehicle (RLV)'s model is highly nonlinear and strong coupling in the respect of input and output variables. Also, the RLV must subject to the boundary constraint, the heat rate constraint, the normal load constraint, the dynamic pressure constraint and so on, and therefore the re-entry trajectory optimization is one of the most challenging problems in the optimal control theory. Many researchers focus on generation and optimization of the RLV's reentry trajectory in the preliminary design[1–3].

Generally, many optimal control problems can not get analytic solutions because they are highly nonlinear. Thus, it is necessary to employ numerical methods to solve the optimal control problems. Numerical methods for trajectory optimization are categorized into direct method and indirect method[4]. In the indirect method, both the calculus of variations and the Pontryagin minimum principle are employed to obtain the first-order optimality conditions[5], and then the solution can be obtained through solving the resulting Hamiltonian boundary-value problem (HBVP) derived from the first-order necessary conditions for optimality[6]. If the problem is solvable, the HBVP produces the costate variables, and thereby we can know how close the solution is to the true optimal solution.

In the direct method[7–9], the state and/or control variables are approximated using a set of basis functions. Then the optimal problem is transcribed to a normal nonlinear programming (NLP) problem, in which variables to be optimized are the coefficients of the basis functions. Compared with the indirect method, the direct method is widely used to solve trajectory optimization problems for the following reasons. Firstly, the convergence radius of the direct method is larger than that of the indirect method[7]. Secondly, it is not necessary to derive optimality conditions in the direct method, whereas it is difficult to derive

Received 3 March 2012; revised 25 October 2012.

[†] Corresponding author. E-mail: hanpeng@bit.edu.cn; Tel.: +86 13810636490.

first-order optimality conditions in the indirect method. Finally, it's much easier to solve the NLP problem than to solve the HBVP arising from the indirect method, because there are numerous well-developed software packages (e.g., SNOPT[10], IPOPT[11], NPSOL[12]) to solve the large sparse NLP problem. However, most of the direct methods can't produce the costate variables from the solution to the NLP problem, and it's difficult to gain insight into the structure of the solution. As a result, it's uncertain whether the solution to the NLP problem is the optimal solution to the trajectory optimization problem.

Over the last decade, the pseudospectral method[13–15], a class of direct methods, has become increasingly popular because costate variables can be mapped from the Karush-Kuhn-Tucker (KKT) multipliers of the NLP problem. In other way, the pseudospectral method combines the best features of both the indirect method and the direct method simultaneously. In the pseudospectral method, the optimal control problem is converted to a NLP problem by parameterizing the state and control variables using global Lagrange or Chebyshev polynomials and collocating the dynamic equations at nodes based on Gaussian quadrature rules. The most well-developed pseudospectral methods are the Lobatto pseudospectral method (LPM), the Gauss pseudospectral method (GPM), and the Radau pseudospectral method (RPM). The three pseudospectral methods differ in the set of collocation points defined on the domain $[-1,1]$. The three sets of collocation points are obtained from the roots of a Legendre polynomial and/or linear combinations of a Legendre polynomial and its derivatives. Reference [16] shows that the GPM and the RPM costate approximations converge exponentially whereas the LPM costate is potentially nonconvergent. In addition, the GPM and the RPM state and control converge at a significantly faster rate as compared with the LPM. Reference [17] comments that the GPM produces oscillating profiles on certain optimal control problems, whereas the RPM leads to much smoother profiles. Because of the inherent stability reasons, the RPM is selected to solve the RLV's re-entry trajectory optimization problem in this paper.

2 Continuous Bolza problem

Consider the following fairly general optimal control problem in Bolza form. Minimize the cost functional

$$J = \Phi(\boldsymbol{x}(\tau_1), t_0, \boldsymbol{x}(\tau_N), t_\mathrm{f}) + \frac{t_\mathrm{f}-t_0}{2}\int_{-1}^{1} \boldsymbol{g}(\boldsymbol{x}(\tau), \boldsymbol{u}(\tau), \tau; t_0, t_\mathrm{f})\mathrm{d}\tau, \quad (1)$$

subject to the dynamic constraints

$$\frac{\mathrm{d}\boldsymbol{x}}{\mathrm{d}\tau} = \frac{t_\mathrm{f}-t_0}{2}\boldsymbol{f}(\boldsymbol{x}(\tau), \boldsymbol{u}(\tau), \tau; t_0, t_\mathrm{f}) \in \mathbb{R}^n, \quad (2)$$

the boundary conditions

$$\phi(\boldsymbol{x}(\tau_1), t_0, \boldsymbol{x}(\tau_N), t_\mathrm{f}) = \boldsymbol{0} \in \mathbb{R}^q, \quad (3)$$

the inequality path constraints

$$\boldsymbol{C}(\boldsymbol{x}(\tau), \boldsymbol{u}(\tau), \tau; t_0, t_\mathrm{f}) \leqslant \boldsymbol{0} \in \mathbb{R}^c, \quad (4)$$

where $\boldsymbol{x}(\tau) \in \mathbb{R}^n$, $\boldsymbol{u}(\tau) \in \mathbb{R}^m$, t are state, control and time variables, respectively. The optimal problem of (1)–(4) can be transformed from the time interval $\tau \in [-1,1]$ to $t \in [t_0, t_\mathrm{f}]$ via the affine transformation

$$t = \frac{t_\mathrm{f}-t_0}{2}\tau + \frac{t_\mathrm{f}+t_0}{2}. \quad (5)$$

3 Radau pseudospectral method

3.1 Legendre-Gauss-Radau collocation points

The RPM is developed based on the Legendre-Gauss-Radau(LGR) collocation points. The LGR collocation points lie on the half open interval $\tau \in [-1,1)$ or $\tau \in (-1,1]$, and contain only one of the points -1 or 1. The LGR points that include the terminal endpoint are often called the flipped LGR points. In this paper, we use the standard set of LGR points, which contains only -1. Denoting n as the number of collocation points, nth degree Legendre polynomial $P_n(\tau)$ is expressed using Rodrigues' formula:

$$P_n(\tau) = \frac{1}{2^n n!}\frac{\mathrm{d}^n}{\mathrm{d}\tau^n}[(\tau^2-1)^n]. \quad (6)$$

The standard LGR points are the roots of $P_{n-1}(\tau)+P_n(\tau)$. A depiction of LGR points is shown in Fig.1. It's noticed from Fig.1 that the LGR points are asymmetric relative to the origin.

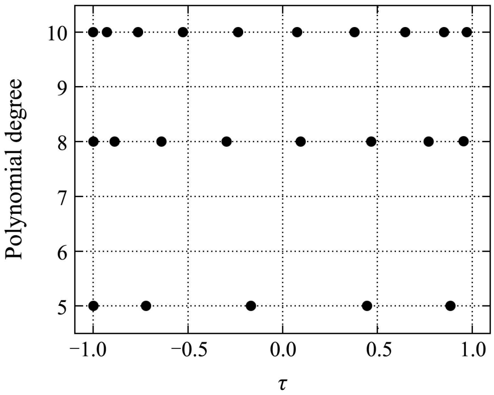

Fig. 1 LGR points ($n = 5, 8, 10$)

3.2 Formulation of Radau pseudospectral method

Let us consider $N-1$ LGR collocation points $\tau_1, \tau_2, \cdots, \tau_{N-1}$ in the interval $\tau \in [-1,1)$ with $\tau_1 = -1$ and $\tau_{N-1} < 1$. An additional noncollocated point $\tau_N = 1$ is introduced to describe the approximation of the state variable. First, the state and control variables are approximated by the following polynomials of degree at most $N-1$ and $N-2$, respectively.

$$\boldsymbol{x}(\tau) = \sum_{i=1}^{N} \boldsymbol{X}_i L_i(\tau),\ i = 1,2,\cdots,N, \quad (7)$$

$$\boldsymbol{u}(\tau) = \sum_{i=1}^{N-1} \boldsymbol{U}_i \tilde{L}_i(\tau),\ i = 1,2,\cdots,N-1, \quad (8)$$

where $\boldsymbol{X}_i$, $\boldsymbol{U}_i$ are approximations of the state and the control at $\tau = \tau_i$, respectively. L_i, $\tilde{L}_i$ are the bases of Lagrange polynomials:

$$L_i(\tau) = \prod_{j=1,j\neq i}^{N} \frac{\tau-\tau_j}{\tau_i-\tau_j}, \quad (9)$$

$$\tilde{L}_i(\tau) = \prod_{j=1,j\neq i}^{N-1} \frac{\tau-\tau_j}{\tau_i-\tau_j}. \quad (10)$$

It's known that L_i, $\tilde{L}_i$ have the properties that

$$L_i(\tau_j)=\begin{cases}1, & i=j\\ 0, & i\neq j\end{cases},\ i,j=1,2,\cdots,N, \tag{11}$$

$$\tilde{L}_i(\tau_j)=\begin{cases}1, & i=j\\ 0, & i\neq j\end{cases},\ i,j=1,2,\cdots,N-1. \tag{12}$$

The time derivative of the state approximation of Eq.(7) is then given as

$$\dot{\boldsymbol{x}}(\tau)=\sum_{i=1}^{N}\boldsymbol{X}_i\dot{L}_i(\tau). \tag{13}$$

Evaluating the result at the kth collocation point τ_k, gives

$$\dot{\boldsymbol{x}}(\tau_k)=\sum_{i=1}^{N}\boldsymbol{X}_i\dot{L}_i(\tau_k)=\sum_{i=1}^{N}D_{ki}\boldsymbol{X}_i, \tag{14}$$

where, $D_{ki}=\dot{L}_i(\tau_k)$, the $(N-1)\times N$ non-square matrix D is called Radau pseudospectral differentiation matrix. For each collocation point k, the matrix has one row, and the element in the ith column is the derivative of the Lagrange polynomials evaluated at the kth collocation point.

The dynamic constraint is transcribed into the algebraic constraint as

$$\sum_{i=1}^{N}D_{ki}\boldsymbol{X}_i-\frac{t_\mathrm{f}-t_0}{2}\boldsymbol{f}(\boldsymbol{X}_k,\boldsymbol{U}_k,\tau_k;t_0,t_\mathrm{f})=0, \tag{15}$$

where, $\boldsymbol{X}_k\equiv\boldsymbol{X}(\tau_k)$, $\boldsymbol{U}_k\equiv\boldsymbol{U}(\tau_k)(k=1,2,\cdots,N-1)$. Note that dynamic constraint is collocated only at the $N-1$ LGR points whereas the state is approximated at the LGR points plus the terminal point $\tau_N=1$.

Then, the continuous-time cost functional of Eq.(1) can be approximated using a Gauss-Radau quadrature, resulting in

$$J=\varPhi(\boldsymbol{X}_0,t_0,\boldsymbol{X}_N,t_\mathrm{f})+\\ \frac{t_\mathrm{f}-t_0}{2}\sum_{k=1}^{N-1}\omega_k\boldsymbol{g}(\boldsymbol{X}_k,\boldsymbol{U}_k,\tau_k;t_0,t_\mathrm{f}), \tag{16}$$

where $\omega_k(k=1,2,\cdots N-1)$ represent the LGR quadrature weights and they are defined as

$$\omega_k=\frac{1-\tau_k}{(N-1)^2[P_{N-2}(\tau_k)]^2}. \tag{17}$$

Furthermore, the boundary conditions of Eq.(3) are also approximated at the boundary points as

$$\phi(\boldsymbol{X}_1,t_0,\boldsymbol{X}_N,t_\mathrm{f})=\boldsymbol{0}. \tag{18}$$

Finally, the path constraints of inequality (4) are enforced at the LGR points as

$$\boldsymbol{C}(\boldsymbol{X}_k,\boldsymbol{U}_k,\tau_k;t_0,t_\mathrm{f})\leqslant\boldsymbol{0},\ k=1,2,\cdots,N-1. \tag{19}$$

The NLP problem that arises from the RPM is then to minimize the cost function of Eq.(16) subjected to the algebraic constraints of Eqs.(15)(18)–(19). And the parameters to be optimized of the NLP problem are the initial time t_0, the final time t_f, the state approximations $\boldsymbol{X}_1,\boldsymbol{X}_2,\cdots,\boldsymbol{X}_N$, and the control approximations $\boldsymbol{U}_1,\boldsymbol{U}_2,\cdots,\boldsymbol{U}_{N-1}$. Reference [18] shows that the KKT conditions of the NLP problem are equivalent to the discretized form of the continuous first order necessary conditions of the continuous Bolza problem when using the Radau pseudospectral discretization. Accordingly, we can get the conclusion that the RPM leads to the ability to determine accurate primal and dual solution to the general optimal control problems.

4 Re-entry modeling

4.1 Equations of motion

During the re-entry phase, the RLV's trajectory is calculated by the following dynamic equations[19], which correspond to the motion over a spherical non-rotating earth:

$$\begin{cases}\dot{v}=-\dfrac{C_\mathrm{x}qS}{m}-g\sin\theta_\mathrm{T},\\ \dot{\theta}_\mathrm{T}=\dfrac{C_\mathrm{L}qS}{mv}\cos\nu-\dfrac{g\cos\theta_\mathrm{T}}{v}+\dfrac{v\cos\theta_\mathrm{T}}{r},\\ \dot{\sigma}_\mathrm{T}=-\dfrac{C_\mathrm{L}qS\sin\nu}{mv\cos\theta_\mathrm{T}}+\dfrac{v\tan\phi\cos\theta_\mathrm{T}\sin\sigma_\mathrm{T}}{r},\\ \dot{\phi}=\dfrac{v\cos\theta_\mathrm{T}\cos\sigma_\mathrm{T}}{r},\\ \dot{\lambda}=-\dfrac{v\cos\theta_\mathrm{T}\sin\sigma_\mathrm{T}}{r\cos\phi},\\ \dot{r}=v\sin\theta_\mathrm{T},\end{cases} \tag{20}$$

where the state variables are velocity v(m/s), flight path angle θ_T(rad), velocity azimuth angle σ_T(rad), geodetic latitude ϕ(rad), longitude λ(rad), geocentric radius r(m). The angle of attack α(rad) and the bank angle ν(rad) are adopted as the control variables. The mass of the RLV is denoted by m(kg), and S(m^2) represents the reference area. C_L, C_x are the aerodynamic lift and drag force coefficients, and they are computed with respect to the angle of attack as

$$C_\mathrm{L}=a_0+a_1\alpha, \tag{21}$$

$$C_\mathrm{x}=b_0+b_1\alpha+b_2\alpha^2. \tag{22}$$

The dynamic pressure is given by $q=1/2\cdot\rho v^2$. The air density ρ is expressed by $\rho=\rho_0\mathrm{e}^{-\beta h}$, here ρ_0 represents the atmospheric density at sea level and h represents the altitude. The acceleration of gravity is modeled by $g=g_0r_0^2/r^2$, here g_0 represents the acceleration of gravity at the sea level, r_0 represents the mean radius of the Earth.

4.2 Re-entry constraints

1) Heat rate constraint: the heating rate on the stagnation regions on the surface of the RLV cannot exceed the limit.

$$q_\mathrm{s}=d_1\sqrt{\rho}(d_2v)^{3.07}(c_0+c_1\alpha+c_2\alpha^2+\\ c_3\alpha^3)\leqslant q_{\mathrm{s\,max}}. \tag{23}$$

2) Normal load constraint: the normal load must be less than the typical limit.

$$n_\mathrm{l}=\sqrt{L^2+D^2}/mg\leqslant n_{\mathrm{l\,max}}, \tag{24}$$

where, the aerodynamic forces, the lift L and the drag D, are given by $L=C_\mathrm{L}qS$, $D=C_\mathrm{x}qS$.

3) Dynamic pressure constraint: an airload constraint based on the dynamic pressure is stated by

$$q=\frac{1}{2}\rho v^2\leqslant q_\mathrm{max}. \tag{25}$$

4) Boundary constraint: the RLV's reentry phase starts at a specified point, ends to get into the terminal area energy management (TAEM) phase. Thus, the states of reentry phase must subject to the boundary constraints.

5) Control variable constraint: the control variables inequality constraints are specified respectively as

$$\begin{cases}\alpha_\mathrm{min}\leqslant\alpha\leqslant\alpha_\mathrm{max},\\ |\nu|\leqslant\nu_\mathrm{max}.\end{cases} \tag{26}$$

4.3 Performance index

The purpose of the research is to find the angle of attack and the bank angle histories to maximize the cross-range. Accordingly, the cost function is

$$J = \max(\text{cross-range}). \tag{27}$$

5 Simulation

5.1 Construction of the NLP

The RLV's aerodynamic and characteristic parameters are based on the space shuttle, and they are cited from Reference [20]. Generally, the initial and final states are specified as

$$\begin{bmatrix} v_0 \\ \theta_{\mathrm{T0}} \\ \sigma_{\mathrm{T0}} \\ \phi_0 \\ \lambda_0 \\ r_0 \end{bmatrix} = \begin{bmatrix} 7803\,\mathrm{m/s} \\ -1^\circ \\ 90^\circ \\ 0^\circ \\ 0^\circ \\ R_\mathrm{e}+79428\,\mathrm{m} \end{bmatrix}, \quad \begin{bmatrix} v_\mathrm{f} \\ \theta_{\mathrm{Tf}} \\ \sigma_{\mathrm{Tf}} \\ \phi_\mathrm{f} \\ \lambda_\mathrm{f} \\ r_\mathrm{f} \end{bmatrix} = \begin{bmatrix} 762\,\mathrm{m/s} \\ -5^\circ \\ \text{free} \\ \text{free} \\ \text{free} \\ R_\mathrm{e}+24384\,\mathrm{m} \end{bmatrix}.$$

Using the same constraints as the ones with the space shuttle, after conversion of English Units to Metric Units, the path constraint limits and control inequality constraints are specified respectively as

$$\begin{bmatrix} q_{\mathrm{s\,max}} \\ n_{\mathrm{l\,max}} \\ q_{\max} \end{bmatrix} = \begin{bmatrix} 794.96\,\mathrm{kJ/(m^2\cdot s)} \\ 2.5 \\ 14.36\,\mathrm{kPa} \end{bmatrix},$$

$$\begin{bmatrix} 10^\circ \\ -80^\circ \end{bmatrix} \leqslant \begin{bmatrix} \alpha \\ \upsilon \end{bmatrix} \leqslant \begin{bmatrix} 40^\circ \\ 80^\circ \end{bmatrix}.$$

There are many ways to define the cross-range, but in this case it is equivalent to maximize the final latitude.

$$J = \max(\text{cross-range}) = \max(\phi_\mathrm{f}). \tag{28}$$

In this case, after the discretization of the re-entry trajectory optimization problem using the RPM described in Section 3, the NLP decision vector $\boldsymbol{z} \in \mathbb{R}^{6n+6}$ is given as

$$\boldsymbol{z} = (t_0, t_\mathrm{f}, \boldsymbol{X}_1, \boldsymbol{X}_2, \cdots, \boldsymbol{X}_{n+1}, \boldsymbol{U}_1, \boldsymbol{U}_2, \cdots, \boldsymbol{U}_n), \tag{29}$$

where, n is a parameter that defines the total number of LGR points, $\boldsymbol{X}_i = (v_i, \theta_{\mathrm{T}i}, \sigma_{\mathrm{T}i}, \phi_i, \lambda_i, r_i)^\mathrm{T}$, $\boldsymbol{U}_i = (\alpha_i, \upsilon_i)^\mathrm{T}$. Obviously, in this case $t_0 = 0$. The objective of the NLP problem is to maximize the cost function

$$J = \max(\boldsymbol{X}_{n+1}(4)). \tag{30}$$

The pseudospectral methods have a larger radius of convergence than other numerical methods, consequently, the RPM does not require a good initial guess. However, an educated initial guess does improve the convergence rate and robustness. Specifically, in this paper, the initial guess for time interval $[t_0, t_\mathrm{f}]$ is $[0, 2000]$. The initial guess for initial state $\boldsymbol{X}_1$ is

$$[7803\,\mathrm{m/s}, -1^\circ, 90^\circ, 0^\circ, 0^\circ, R_\mathrm{e} + 79428\,\mathrm{m}]^\mathrm{T},$$

and for final state $\boldsymbol{X}_{n+1}$ is

$$[762\,\mathrm{m/s}, -5^\circ, 90^\circ, 0^\circ, 0^\circ, R_\mathrm{e} + 24384\,\mathrm{m}]^\mathrm{T}.$$

It is noted that the desired $\boldsymbol{X}_{n+1}(3 \sim 5)$ is free, and thereby we choose the initial guess for $\boldsymbol{X}_{n+1}(3 \sim 5)$ is $\boldsymbol{X}_1(3 \sim 5)$. For a LGR collocation point t in the time interval $[t_0, t_\mathrm{f}]$, the initial guess for the state variable of this point is obtained by the linear interpolation method. The initial guesses for all control variables $\boldsymbol{U}_i (i = 1, 2, \cdots, n)$ are 0.

The NLP problem is then solved using the software package SNOPT for $n = 40$ to $n = 110$, and the SNOPT optimality and feasibility tolerances are 10^{-6}. All computations are performed using a 2.10GHz/Intel Core i3-2310M CPU running 64-bit Windows 7 with MATLAB 2012a.

5.2 Discussion of the results

Table 1 and Table 2 show the summaries of result using the RPM and the GPM respectively. Theoretically, the more collocation points we employ, the more accurate approximation we can get. However, too many collocation points can lead to too much time to solve the arising NLP problem. Table 1 and Table 2 show that the RPM can run very faster than the GPM when using the same number of collocation points, and the gap between the two methods grows when the number of collocation points increases.

Table 1 Summary of result using the RPM

n	CPU time/s	t_f/s	$\phi_\mathrm{f}/(^\circ)$
40	3.95	2198.82	30.642560
50	6.61	2198.79	30.644474
60	9.58	2200.23	30.644686
70	10.41	2199.53	30.644447
80	16.75	2199.72	30.644559
90	24.35	2200.17	30.644278
100	35.05	2199.62	30.644221
110	49.37	2199.69	30.644286

Table 2 Summary of result using the GPM

n	CPU time/s	t_f/s	$\phi_\mathrm{f}/(^\circ)$
40	4.14	2199.08	30.645765
50	7.29	2200.36	30.644832
60	13.09	2199.99	30.643852
70	19.84	2199.33	30.644160
80	34.45	2199.89	30.644323
90	51.10	2199.60	30.644292
100	83.20	2199.55	30.644415
110	100.74	2199.95	30.644367

The control variable histories obtained via 60 LGR points are illustrated in Fig.2 and Fig.3. The controls are seen to remain within their specified limitations. The optimal state variables (altitude, velocity, longitude, latitude, flight path angle and velocity azimuth angle) are displayed in Figs.4–9, respectively. The circles present the state approximations obtained by the RPM in 60 collocation points, and the solid lines show the state histories from integrating the differential dynamic equations in Eq.(20) with the optimal open-loop controls in Fig.2 and Fig.3. Figs.10–12 are provided to show the path constraints. The circles and the lines in Figs.10–12 have the same meanings with those in Figs.4–9. The states and constraints are nearly a perfect match. As seen from Fig.10 and Fig.11, the dynamic pressure and the normal load are low at the beginning of the reentry, and they increase gradually with time. However, the dynamic pressure constraint and the normal load constraint are inactive during the whole reentry phase. Fig.12 shows that the boundary contact first occurs with the heat rate constraint at about 80 s. However, the heat rate is controlled within a specified limit. The little difference between the circles and the lines shows the high precision of the RPM.

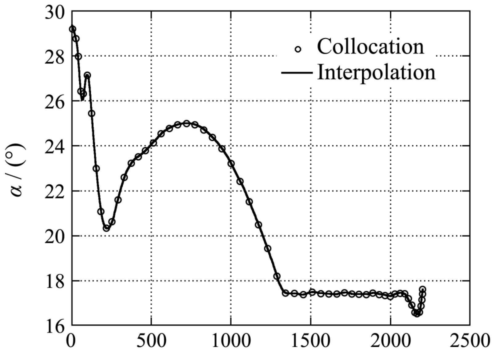

Fig. 2 Angle of attack profile

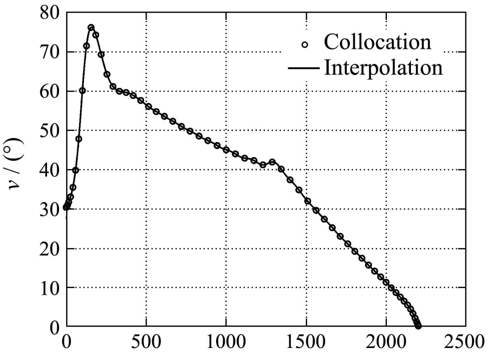

Fig. 3 Bank angle profile

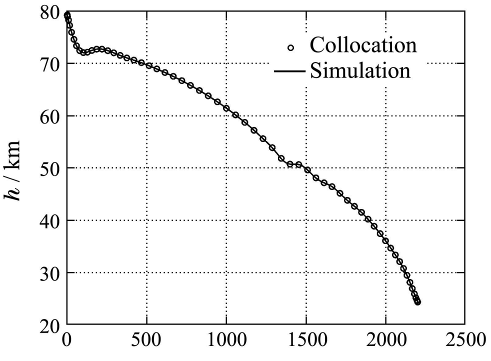

Fig. 4 Altitude profile

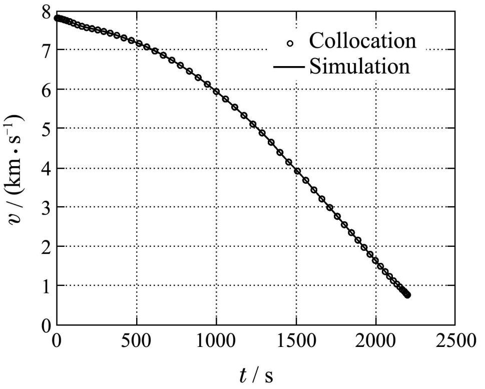

Fig. 5 Velocity profile

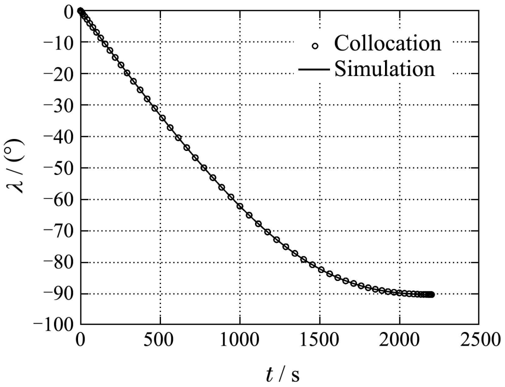

Fig. 6 Longitude profile

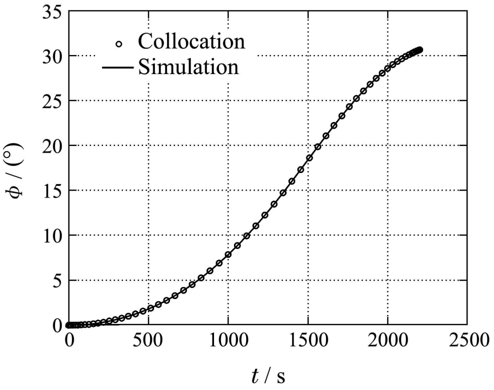

Fig. 7 Latitude profile

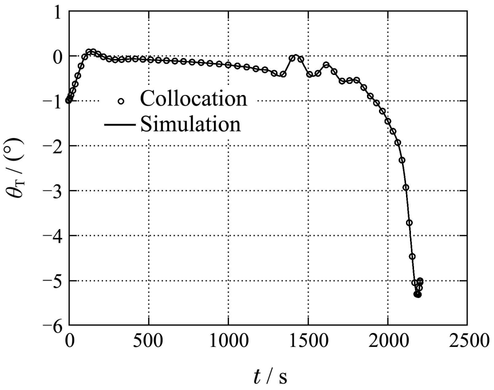

Fig. 8 Flight path angle profile

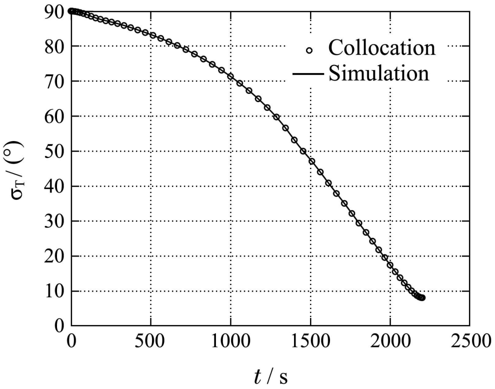

Fig. 9 Velocity azimuth angle profile

The terminal states of simulation are $v_f = 762.42$ m/s, $\theta_{Tf} = -4.999°$, $r_f = R_e + 24390.48$ m. The peak values of heating rate, dynamic pressure, and normal load are

799.77 kJ/(m$^2\cdot$s), 12.54 kPa, and 1.18, respectively. Simulation results show that the optimized re-entry trajectories satisfy the boundary constraints and the path constraints in an acceptable tolerance range.

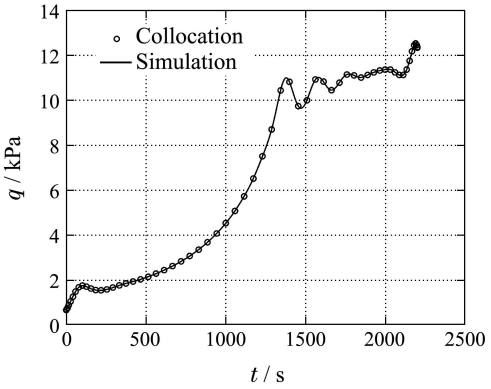

Fig. 10 Dynamic pressure profile

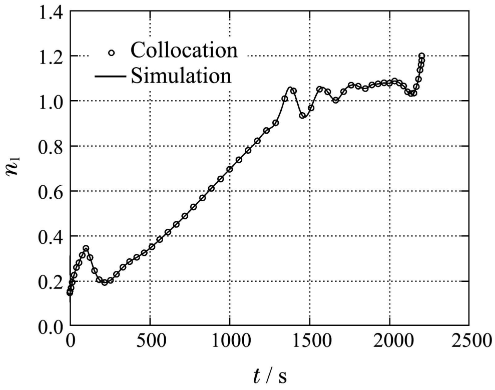

Fig. 11 Normal load profile

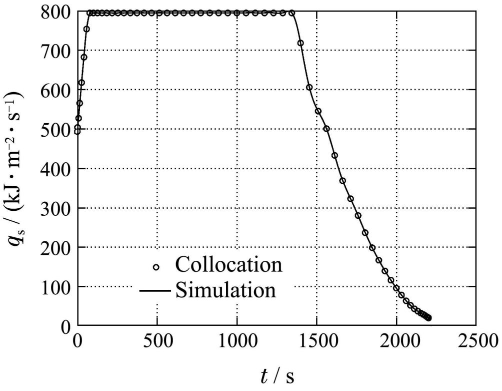

Fig. 12 Heat rate profile

6 Conclusions

A method has been presented for RLV's re-entry trajectory optimization. The optimal control problem is transcribed to a NLP problem by parameterizing the state and control using global polynomials and collocating the differential-algebraic equations at LGR points. Simulation results show that the optimized re-entry trajectories satisfy the boundary constraints and the path constraints successfully. When comparing with the GPM, it is found that the RPM is more efficient computationally. Because of its high efficiency and high precision, we can indicate that the RPM can be used for real-time trajectory generation.

References:

[1] LEE D. Optimization analysis of trajectory for re-entry vehicle using global orthogonal polynomial [J]. *Journal of Mechanical Science and Technology*, 2006, 20(10): 1557 – 1566.

[2] UNDURTI A, PROULX R J, SHEARER J A, et al. Optimal trajectories for maneuvering re-entry vehicles [J]. *Advances in the Astronautical Sciences*, 2008, 129(1): 879 – 900.

[3] JORRIS T R, SCHULZ C S, REXIUS S. Improvements in pseudospectral based hypersonic vehicle trajectory generation via enhanced aerothermal prediction methods [J]. *Spaceflight Mechanics*, 2009, 134(3): 1777 – 1791.

[4] BETTS J T. Survey of numerical methods for trajectory optimization [J]. *Journal of Guidance Control and Dynamics*, 1998, 21(2): 193 – 207.

[5] HULL D G. *Optimal Control Theory for Applications* [M]. Berlin: Springer-Verlag, 2003.

[6] RAO A V. A survey of numerical methods for optimal control [J]. *Astrodynamics*, 2009, 135(1): 497 – 528.

[7] ROH W, KIM Y. Trajectory optimization for a multi-stage launch vehicle using time finite element and direct collocation methods [J]. *Engineering Optimization*, 2002, 34(1): 15 – 32.

[8] TU L, YUAN J, YUE X, et al. Improving design of reentry vehicle trajectory optimization using direct collocation method [J]. *Journal of Northwestern Polytechnical University*, 2006, 24(5): 653 – 657

[9] TANG S, CONWAY B A. Optimization of low-thrust interplanetary trajectories using collocation and nonlinear-programming [J]. *Journal of Guidance Control and Dynamics*, 1995, 18(3): 599 – 604.

[10] GILL P E, MURRAY W, SAUNDERS M A. SNOPT: an SQP algorithm for large-scale constrained optimization [J]. *SIAM Review*, 2005, 47(1): 99 – 131.

[11] BIEGLER L T, ZAVALA V M. Large-scale nonlinear programming using IPOPT: an integrating framework for enterprise-wide dynamic optimization [J]. *Computers & Chemical Engineering*, 2009, 33(3): 575 – 582.

[12] HOLMSTROM K, GORAN A O, EDVALL M M. *User's Guide for TOMLAB/NPSOL* [EB/OL]. Seattle: TOMLAB, 2008-2-13 [2012-3-3]. http://tomopt.com/docs/TOMLAB_NPSOL.pdf.

[13] RAO A V, GARG D, HAGER W W. Pseudospectral methods for solving infinite-horizon optimal control problems [J]. *Automatica*, 2011, 47(4): 829 – 837.

[14] LI J S, RUTHS J, STEFANATOS D. A pseudospectral method for optimal control of open quantum systems [J]. *Journal of Chemical Physics*, 2009, 131(16): 2009, 131(16): 164110 – 164118.

[15] KANG W. Rate of convergence for the Legendre pseudospectral optimal control of feedback linearizable systems [J]. *Journal of Control Theory and Applications*, 2010, 8(4): 391 – 405.

[16] GARG D, PATTERSON M, HAGER W W, et al. A unified framework for the numerical solution of optimal control problems using pseudospectral methods [J]. *Automatica*, 2010, 46(11): 1843 – 1851.

[17] BAUSA J, TSATSARONIS G. Dynamic optimization of startup and load-increasing processes in power plants, Part I: method [J]. *Journal of Engineering for Gas Turbines and Power*, 2001, 123(1): 246 – 250.

[18] GARG D, PATTERSON M A, FRANCOLIN C, et al. Direct trajectory optimization and costate estimation of finite-horizon and infinite-horizon optimal control problems using a Radau pseudospectral method [J]. *Computational Optimization and Applications*, 2011, 49(2): 335 – 358.

[19] ZHAO Hanyuan. *Reentry Flight Vehicle Dynamics and Guidance* [M]. Changsha: National University of Defense Technology Press, 1997.
(赵汉元. 飞行器再入动力学和制导 [M]. 长沙: 国防科技大学出版社, 1997.)

[20] BETTS J T. *Practical Methods for Optimal Control Using Nonlinear Programming* [M]. Philadelphia: Society for Industrial Mathematics, 2001.

作者简介:

韩 鹏 (1985–), 男, 博士研究生, 目前研究方向为飞行器轨迹优化、制导与控制, E-mail: hanpeng@bit.edu.cn;

单家元 (1967–), 男, 教授, 目前研究方向为飞行器制导、控制与仿真, E-mail: sjy1919@bit.edu.cn.